

SEARCH FOR NON-GAUSSIAN SIGNALS IN THE BOOMERANG MAPS: PIXEL-SPACE ANALYSIS

G. POLENTA¹, P.A.R. ADE², J.J. BOCK³, J.R. BOND⁴, J. BORRILL⁵, A. BOSCALERI⁶,
C.R. CONTALDI⁴, B.P. CRILL⁷, P. DE BERNARDIS¹, G. DE GASPERIS⁸, G. DE TROIA¹,
K. GANGA⁹, M. GIACOMETTI¹, E. HIVON⁹, V.V. HRISTOV⁷, A.H. JAFFE¹⁰, A.E. LANGE⁷,
S. MASI¹, P.D. MAUSKOPF¹¹, A. MELCHIORRI¹², T. MONTROY¹³, P. NATOLI⁸,
C.B. NETTERFIELD¹⁴, E. PASCALE⁶, F. PIACENTINI¹, D. POGOSYAN⁴, S. PRUNET⁴, G. ROMEO¹⁵,
J.E. RUHL¹³, N. VITTORIO⁸, A. ZEPPELLI¹

¹ Dipartimento di Fisica, Universita' La Sapienza, Roma, Italy

² Queen Mary and Westfield College, London, UK

³ Jet Propulsion Laboratory, Pasadena, CA, USA

⁴ Canadian Institute for Theoretical Astrophysics, University of Toronto, Canada

⁵ National Energy Research Scientific Computing Center, LBNL, Berkeley, CA, USA

⁶ IROE-CNR, Firenze, Italy

⁷ California Institute of Technology, Pasadena, CA, USA

⁸ Dipartimento di Fisica, Universita' Tor Vergata, Roma, Italy

⁹ IPAC, California Institute of Technology, Pasadena, CA, USA

¹⁰ Astrophysics Group Blackett Laboratory, Imperial College, London, UK

¹¹ Dept. of Physics and Astronomy, Cardiff University, Cardiff CF24 3YB, Wales, UK

¹² Nuclear and Astrophysics Laboratory, University of Oxford, Keble Road, Oxford, OX 3RH, UK

¹³ Dept. of Physics, Univ. of California, Santa Barbara, CA, USA

¹⁴ Depts. of Physics and Astronomy, University of Toronto, Canada

¹⁵ Istituto Nazionale di Geofisica, Roma, Italy

Jan. 9, 2002

ABSTRACT

We search the BOOMERanG maps of the anisotropy of the Cosmic Microwave Background (CMB) for deviations from gaussianity. In this paper we focus on analysis techniques in pixel-space, and compute skewness, kurtosis and Minkowski functionals for the BOOMERanG maps and for gaussian simulations of the CMB sky. We do not find any significant deviation from gaussianity in the high galactic latitude section of the 150 GHz map. We do find deviations from gaussianity at lower latitudes and at 410 GHz, and we ascribe them to Galactic dust contamination. Using non-gaussian simulations of instrumental systematic effects, of foregrounds, and of sample non-gaussian cosmological models, we set upper limits to the non-gaussian component of the temperature field in the BOOMERanG maps. For fluctuations distributed as a 1 DOF χ^2 mixed to the main gaussian component our upper limits are in the few % range.

Subject headings: Cosmic Microwave Background Anisotropy, Cosmology

1. INTRODUCTION

In most inflationary scenarios the primordial density field is expected to be gaussian (see e.g. Peebles 1999). In contrast, structure formation scenarios based on topological defects (e.g. Avelino et al. 1998) or less general inflationary models (Linde et al. 1997; Martin et al. 2000; Contaldi et al. 1999) predict a non-gaussian density field. Thus, measurement of the statistical nature of the CMB anisotropies can distinguish between these scenarios (see e.g. Fischler et al. 1985).

The presence of noise in the measurements combined with the limited coverage of the present observations can mask cosmological non-gaussian features. Moreover, the presence of systematic effects can produce subtle instrumental non-gaussian features in intrinsically gaussian anisotropy maps.

Efforts to identify non-gaussianities in the CMB have been extensively carried out for the COBE data (see e.g. Ferreira et al. 1998; Banday et al. 1999; Komatsu et al. 2001; Bromley and Tegmark 2000) and no significant detection of cosmological non-gaussianity has been reported (but see Magueijo 2000). However, the sensitivity of COBE-DMR to the expected levels of cosmo-

logical non-gaussianity from rare highly non-linear events like topological defects (see e.g. Durrer and Zhou 1996) is not very high, due to the large field of view which smears out the effects of small scale features. While the present observations on the power spectrum are inconsistent with a structure formation scenario solely based on defects (see e.g. Durrer et al. 1998), a mixed inflation+defects model is still compatible with the data (Bouchet et al. 2001).

Furthermore, the low signal-to-noise ratio and coarse resolution in the COBE maps also makes it difficult to detect primordial non-gaussianity; the central-limit theorem states that the sum of various instrumental effects will make the distribution tend to a gaussian (Novikov et al. 2000).

Analyses to date of higher angular resolution experiments, like QMASK (Park et al. 2001) and MAXIMA (Santos et al. 2001; Wu et al. 2001), show full consistency with gaussianity.

In this paper we focus on the maps produced by the BOOMERanG experiment (de Bernardis et al 2000; Netterfield et al. 2001). Due to its wide sky and frequency coverage, BOOMERanG is ideally suited to carry out an

accurate analysis of the possible systematic effects present in the detected signal. We analyze them using a Monte-Carlo approach, in order to set quantitative upper limits for the level of primordial non-gaussian fluctuations present in the maps.

The data we use are presented in section 2. We use five estimators of departures from gaussianity: the skewness and kurtosis of the CMB temperature distribution, and the three Minkowski functionals: area, length and genus (Minkowski 1903). In section 3 we apply these estimators to the BOOMERanG maps and to gaussian Monte-Carlo simulations of the CMB sky observed by BOOMERanG. In section 4 we analyze template maps of other non-gaussian signals which could in principle be present in the BOOMERanG maps; we study how sensitive the pixel-space techniques are in detecting these effects, and we estimate how much these affect the measurements of cosmological non-gaussian signals. In section 5 we compare our measurements to the cosmological expectations for a few sample scenarios.

The methods presented here are especially useful in the detection of highly non-linear features (as expected in topological defects theories or for Galactic foregrounds) (Phillips and Kogut 2001). One may alternatively use a wavelets approach (Hivon et al. 2002), or a bispectrum approach (Contaldi et al. 2002).

2. THE DATA

We use the BOOMERanG data obtained in the Long Duration Balloon (LDB) flight in 1998. For this paper we try to be as conservative as possible, so we concentrate on the center of the map, 1.19% of the full sky ($70^\circ < \text{RA} < 105^\circ$, $-55^\circ < \delta < -35^\circ$), where the sky coverage is approximately uniform and the integration time per pixel is maximum. The galactic latitude of this region spans from -42° to -13° . This box contains $37480 7' \times 7'$ pixels in the HEALPix pixelisation (Górski et al. 1998). We also consider for comparison a lower latitude region with similar size but extending to $b < -5^\circ$. We concentrate on the best 150 GHz channel, B150A, for CMB signals, and on the best 410 GHz channel, B410B1, for monitoring the dust foreground. We use only data collected in 1dps scans. The best fit dipole anisotropy component is removed from the time ordered data (TOD) before further processing. TOD are deconvolved from the frequency response of the instrument and high-pass filtered with a sharp filter, with a cut-on at 70 mHz. We use the improved pointing solution of (Netterfield et al. 2001), featuring an equivalent beam FWHM of $12.7'$ for the B150A channel. The time ordered data obtained in this way are converted into a map using the fast iterative generalized least squares map making of (Natoli et al. 2001). The time-domain high-pass filtering procedure removes most of the $1/f$ noise and most of the scan-synchronous noise (SSN, see section 4), but also introduces an important anisotropy in the large-scale content of the map: large scale components of the sky temperature distribution are filtered out in directions parallel to the scan, while being maintained in directions orthogonal to the scan. This is not completely recovered by the map making. Since the scan direction is not constant during the flight, it is difficult to model analytically the effect of such a filter. For

this reason all the subsequent analysis is performed numerically, using Monte-Carlo techniques.

3. ANALYSIS OF THE MAPS

The normalized skewness S_3 and kurtosis S_4 are computed from the 2^{nd} , 3^{rd} and 4^{th} moments $\sigma^2 = \sum_i (T_i - \langle T \rangle)^2 / (N - 1)$, $\mu_3 = \sum_i (T_i - \langle T \rangle)^3 / N$ and $\mu_4 = \sum_i (T_i - \langle T \rangle)^4 / N$ of the distribution of the T_i : $S_3 = \mu_3 / \sigma^3$, $S_4 = \mu_4 / \sigma^4 - 3$. We find $S_3 = -0.03$ and $S_4 = 0.19$. These values are plotted as vertical lines in fig.1. As a comparison, the 410 GHz channel in the same region produces $S_3 = -0.04$ and $S_4 = 0.66$. Due to the presence of sample variance, as well as noise, correlations and anisotropic filtering, these values are not expected to be zero, even for a perfectly gaussian sky. For this reason we compare the measured data to Monte-Carlo simulations. These are based on gaussian maps of the CMB sky extracted from a parent distribution with the best fit power spectrum measured by BOOMERanG (Netterfield et al. 2001). These maps are sampled along the BOOMERanG scans, simulated noise with the statistical properties of the considered channel is added, and the resulting TOD is filtered in the same way as the BOOMERanG data. We then obtain simulated observed maps using the same algorithm we have used for the actual BOOMERanG signals. From each simulated map we compute S_3 and S_4 , and plot their distribution in fig.1a and 1b. The visual comparison of the actual measurement to the simulations suggests consistency with a gaussian sky at 150 GHz. From the distributions we obtain that for the 150 GHz channel S_3 and S_4 differ from the average by 0.8σ and 1.7σ respectively, while for the 410 GHz channel they differ by 1σ and 6σ respectively. In the region at lower Galactic latitudes S_3 and S_4 differ from the average by 3.5σ and 1.0σ (150 GHz) and 7σ and 28σ (410 GHz) respectively.

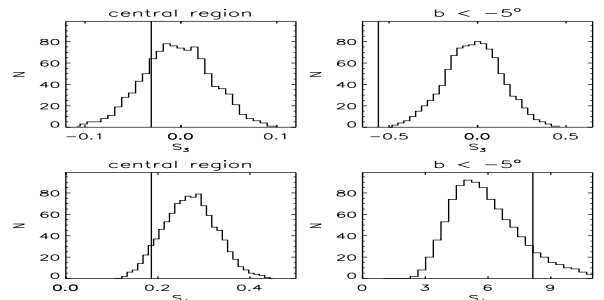


FIG. 1. Measured values of the normalized skewness (top) and kurtosis (bottom) in the nominal box (left) and in the low latitudes box (right) at 150 GHz are shown as vertical lines. The histograms are computed from detailed Monte-Carlo simulations of the measurements. The simulations were obtained from a combination of a gaussian sky with the best fit power spectrum measured in B98 and a simulation of detector noise. The different shape of the distributions is due to uneven coverage and noise per pixel.

For a given threshold ν we compute the surface densities of three Minkowski functionals v_j from the contours ∂Q of the excursion sets $Q \equiv Q(\nu) = \{T_i : (T_i - \langle T \rangle) / \sigma > \nu\}$ (see e.g. Gott et al. 1990):

$$v_0 = \frac{1}{A} \int_Q dA, \quad v_1 = \frac{1}{4A} \int_{\partial Q} ds, \quad v_2 = \frac{1}{2\pi A} \int_{\partial Q} kds \quad (1)$$

where dA and ds are the differential elements of Q and ∂Q respectively, and k is the geodesic curvature of ds . The values of the v_j measured from the 150 GHz map are plotted in fig.2. Again, even for a gaussian sky, the presence of noise, correlations and anisotropic filtering does not allow us to compare the measurements to the analytic expressions of v_j which can be computed for gaussian isotropic distributed data. So we compute the distributions of the v_j from the simulated maps. We plot the 95% confidence band of the v_j vs threshold ν in fig.2. The consistency of the measured v_j with the gaussian sky hypothesis is evident.

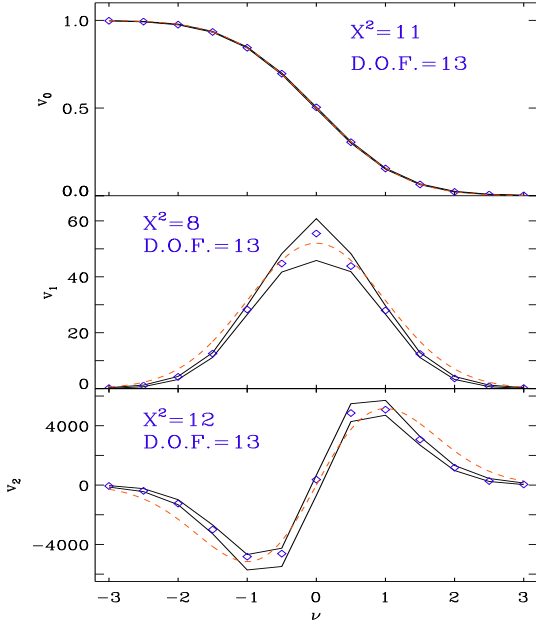


FIG. 2. Measured values of the area (top), length (middle) and genus (bottom) Minkowski functionals in the nominal box at 150 GHz are plotted as diamonds vs the normalized threshold. The solid lines represent the 95% confidence band of the distributions of the same quantities as computed from detailed Monte-Carlo simulations of the measurements obtained assuming a purely gaussian sky with the best fit power spectrum measured in B98, and a realistic simulation of detector noise. Dashed lines are analytical predictions for the gaussian isotropic case.

To compare numerically the measured Minkowski functionals to the simulations, we define a $\chi_j^2 = \sum_\nu [v_j^{obs}(\nu) - \langle v_j^{sim}(\nu) \rangle]^2 / \sigma^2(v_j(\nu))$. From the Monte-Carlo simulations we verified that the variables χ_j^2 are actually distributed as χ^2 with 13 DOF. From the measured data we have $\chi_0^2 = 11$, $\chi_1^2 = 8$, $\chi_2^2 = 12$. So we have $P(\chi^2 > \chi_0^2) = 61\%$, $P(\chi^2 > \chi_1^2) = 84\%$, $P(\chi^2 > \chi_2^2) = 53\%$: again an excellent agreement with the gaussian sky hypothesis. As a comparison, for the 410 GHz data we have $\chi_0^2 = 16$, $\chi_1^2 = 12$, $\chi_2^2 = 162$, $P(\chi^2 > \chi_0^2) = 25\%$, $P(\chi^2 > \chi_1^2) = 53\%$, $P(\chi^2 > \chi_2^2) < 10^{-8}$. In the low Galactic latitudes box the Gaussian hypothesis is rejected for all the functionals, for both the 150 GHz channel and the 410 GHz channel.

4. ESTIMATES OF SYSTEMATIC EFFECTS

Though we do not detect any evidence for non-gaussianity in the maps, we set upper limits on possible sources of non-cosmological non-gaussianity in order to assess the potential for further analysis using more data. The raw BOOMERanG TOD are affected by a large scale SSN, typically of the order of $20 \mu K^\circ$ in the 150 GHz channels and of $400 \mu K^\circ$ (CMB temperature units) in the 410 GHz channels. The delay between the SSN and the azimuth observed suggests an instrumental, thermal origin of the SSN. We have subtracted the best fit CMB dipole from the 150 GHz TOD and low passed the TOD to keep only the large scale SSN. We have then built a map from this signal with the usual map making algorithm, including the high pass filter, which strongly reduces the SSN amplitude (see fig.3). Despite the relatively large signal in the TOD, the anisotropies induced in the filtered map are of the order of few μK in the central box considered for this analysis.

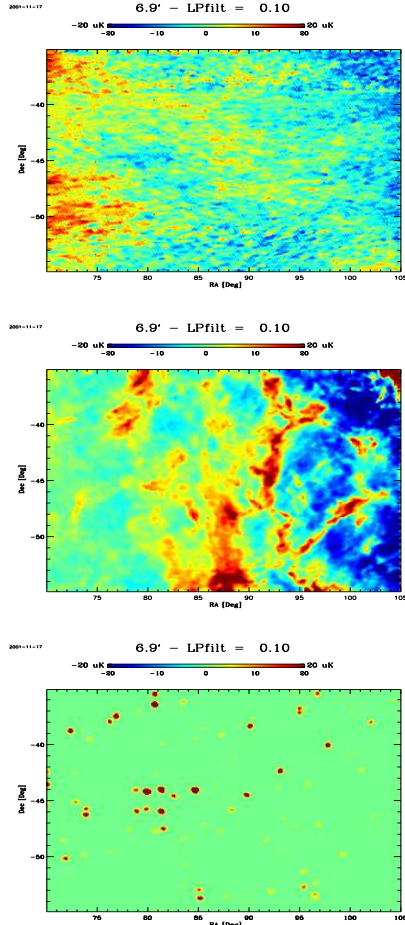


FIG. 3. Estimated systematic effects at 150 GHz in the observed sky region. The top panel shows the effect of Scan Synchronous Noise (SSN) when projected on the sky using the same map-making procedure used for the actual data. The middle panel represents the extrapolation of interstellar dust emission from the FSD maps. The bottom panel shows the expected signal from extragalactic point-sources extrapolated at 150 GHz using the WOMBAT catalogue. For visualisation 0.1° cut-off low-pass filter has been applied to all the maps.

These are very small with respect to the detected anisotropies, but evidently non-gaussian. We have used this map as a template of a systematic effect. We built simulations of contaminated data by adding this map to the gaussian simulations of the CMB used in section 3. Then we have applied our gaussianity estimators to the simulated maps. The result is that the distributions of the estimators are not affected by the presence of SSN at the level we had in the 150 GHz channel analyzed here. We compare the χ^2 of the gaussian-only simulations defined above to the χ^2 of the contaminated simulations, for different levels of the SSN map. We find that the mean square amplitude of the SSN fluctuations should be of the order of 30 to 50% of the mean square CMB fluctuations (depending on the estimator) before becoming detectable. This means that the SSN contribution would have to be at least 8 times larger than that actually observed to affect the results reported in section 3.

The second source of a systematic effect we have considered is thermal emission from interstellar dust. We have used the FSD maps (Finkbeiner et al. 1999) filtered as in (Masi et al. 2001) to produce a template 150 GHz dust map. This is strongly non-gaussian, as visible in fig.3, but its level is very small with respect to the general level of CMB anisotropy. We have added this map to the gaussian CMB simulations, and applied our gaussianity tests. Again, the χ^2 and the distributions of the contaminated simulations are very close to those of the gaussian-only simulations. Interstellar dust emission would have to be 3 times larger than the FSD prediction to contaminate the results reported in section 3.

The third source of a systematic effect we have considered is emission from extragalactic sources present in the observed region. We have used the WOMBAT catalogue (2001) to extrapolate to 150 GHz the flux of known radio sources in the surveyed area. From the catalogue obtained in this way we create a map convolving the point-source flux with the angular response of our telescope. The map (fig.3) — which is evidently non-gaussian — is added to the gaussian CMB simulations and the analysis with our estimators is carried out. Yet again, the χ^2 and the distributions of the contaminated simulations are very close to those of the gaussian-only simulations. Fluxes from extragalactic sources would have to be 30 times larger than the WOMBAT predictions to contaminate the results reported

in section 3.

5. COSMOLOGICAL SOURCES OF NON GAUSSIANITY

There are many models of non-gaussian CMB fluctuations. We have considered a few which can be easily compared to our results. As a first concrete example, we have used Linde's model (Linde et al. 1997). In this case CMB fluctuations are distributed as a χ^2 with 1 DOF. This hypothesis is strongly rejected by all of our estimators. In other models there is a mixture of gaussian and non-gaussian CMB anisotropies (e.g. (Bouchet et al. 2001)). For example, Lyth and Wands ((2001)), consider a mixture of 1 DOF χ^2 distributed fluctuations with Gaussian CMB anisotropies. From Monte Carlo simulations we find that the 95% confidence upper limits to the rms amplitude of the non-Gaussian signal are 2%, 5% and 8% of the Gaussian one (using Area, Length and Genus Minkowski estimators respectively). We have also simulated CMB maps with a specified (equal- ℓ reduced) bispectrum $B_\ell = AC_\ell^{3/2}$ (see (Contaldi and Magueijo 2001)). For C_ℓ we used the B98 best fit power spectrum. For the non-Gaussianity estimators considered in this paper, we detected no deviation from Gaussianity significant at the 95% CL over the range of amplitudes A from 0 to 10.

6. CONCLUSIONS

The pixel-based techniques discussed here and applied to the central region observed by BOOMERanG at 150 GHz confirm the Gaussianity of the detected CMB fluctuations, and exclude with high confidence χ^2 distributed CMB temperature fluctuations. These techniques also detect non-Gaussian fluctuations due to interstellar dust at high frequencies and at lower latitudes. Subdominant non-Gaussian fluctuations mixed to the Gaussian ones are strongly excluded for some models, while are not detected at all in other cases.

The BOOMERanG project has been supported by Programma Nazionale di Ricerche in Antartide, Universit di Roma “La Sapienza”, and Agenzia Spaziale Italiana in Italy, by NASA and by NSF OPP in the U.S., by PPARC in the UK, and by the CIAR and NSERC in Canada. We acknowledge the use of the HEALPix package.

REFERENCES

Avelino P.P., Shellard E.P.S., Wu J.H.P., and Allen B. 1998, Ap.J., 507, L101.
 Banday A. et al. 1999, Ap.J., 533, 575.
 Bouchet F.R. et al. 2001, astro-ph/0005022.
 Bromley B.C., and Tegmark M. 2000, Ap.J., 524, L79.
 Contaldi C.R., Bean and Magueijo J. 1999, Phys. Lett. B468, 189.
 Contaldi C.R. and Magueijo J. 2001, PRD in press, astro-ph/0101512.
 Contaldi C.R. et al., in preparation, paper III.
 de Bernardis P. et al., 2000, Nature, 404, 955.
 Durrer R., and Zhou Z.H. 1996, Phys. Rev. D 53, 5394.
 Durrer R., Kunz M., and Melchiorri A. 1998, Phys. Rev. D V59, 123005.
 Ferreira P.G., Magueijo J., Gorski K.M., Ap.J., 503, L1, 1998.
 Finkbeiner D.P. et al. 1999, Ap.J., 524, 867.
 Fischler W., et al. 1985, Nucl. Phys. B, 259, 730.
 Gorski, K.M., Hivon, E. and Wandelt, B.D., 1998, astro-ph/9812350; <http://www.eso.org/kgorski/healpix/>
 Gott J.R. et al., 1990, Ap.J., 352, 1.
 Hivon E. et al., in preparation, paper II

Komatsu E., et al., 2001, astro-ph/0107605.
 Linde A., Mukhanov V., 1997, Phys. Rev., D56, 535-539.
 Lyth D. & Wands D., 2001, hep-ph/0110002.
 Magueijo J., 2000, Ap.J., 528, L57.
 Martin J., Riazuelo A. and Sakellariadou M. 2000, Phys. Rev. D 61, 083518.
 Masi S., et al. 2001, Ap.J., 553, L93-L96.
 Minkowski H., 1903, Math. Ann. 57, 447.
 Natoli P., et al. 2001, A&A, vol. 371, pag. 346, 2001, astro-ph/0101252.
 Netterfield C.B., et al. 2001, submitted to Ap.J., astro-ph/0104460.
 Novikov D., Schmalzing J., and Mukhanov V. 2000, astro-ph/0006097.
 Park C. et al. 2001, submitted to Ap.J., astro-ph/0102406.
 Peebles P.J.E. 1999, Ap.J., 510, 523.
 Phillips N.G., and Kogut A. 2001, Ap.J., 548, 540.
 Santos M.G. et al., 2001, astro-ph/0107588.
 WOMBAT: <http://astron.berkeley.edu/wombat/foregrounds/radio.html>
 Wu J.H.P. et al., 2001, astro-ph/0104248